Journal of Visualization, Vol. 7, No. 4 (2004) 281-289

Analysis of Submerged Water Jets by Visualization Method

Flow Pattern and Self-Induced Vibration of Jet

Shimada, N.[*1], Hibara, H.[*2], Ishibashi, Y.[*3], Sumida, M.[*4] and Sudo, K.[*5]

*1 Chair of Maritime Safety Technology, Japan Coast Guard Academy, 5-1 Wakaba-cho, Kure, Hiroshima 737-8512, Japan. Tel:+81-823-21-4961/Fax:+81-823-20-0087, E-mail: shimada@jcga.ac.jp
*2 Faculty of Engineering, Ehime University, 3 Bunkyo-cho, Matsuyama, Ehime 790-8577, Japan.
*3 Chiba Polytechnic College, 221-20 Namiki-cho, Narita, Chiba 286-0045, Japan.
*4 Graduate School of Engineering, Hiroshima University, 1-4-1 Kagamiyama, Higashi-Hiroshima, Hiroshima 739-8527, Japan.
*5 Shibaura Institute of Technology, 3-9-14 Shibaura, Minato-ku, Tokyo 108-8548, Japan.

Received 26 August 2003
Revised 6 April 2004

Abstract : This paper is concerned with an experimental investigation on plane submerged water jets discharged into quiescent water in an open channel. Flows are visualized by using hydrogen bubbles, solid particles and dye. The results show that the jets attaching to the water surface by the Coanda effect are classified into six types according to their behavior after issuing from the nozzle, and that the self-induced vibration of the jet, which is one of six flow patterns, occurs under the condition of the reduced Froude number $Fr^* \fallingdotseq 0.7 \sim 1.0$. An additional analysis of the photographs reveals that the self-induced vibration of the jet is caused by attachment of the jet to the water surface and the ensuing bifurcation of the jet at an attachment point, and that the frequency of vibration is independent of the water level.

Keywords : Flow Visualization, Hydraulic Jump, Self-Induced Vibration, Water Jet.

1. Introduction

In engineering we often encounter cases in which a water jet is propagated through an open channel, such as in the case of water jets from sluice gates, dams, and manufacturing or waterpower plants. A simplified diagram of the propagation of a jet in an open channel is given in Fig. 1, which shows the longitudinal section of a channel; a jet is discharged into the channel at the dead end with an initial thickness of the jet h and with a constant velocity Uo ; the other end of the channel has a weir. As we move away from the initial section AA', the thickness of the zone in which the jet mixes with the surrounding water is enlarged, and the constant velocity core in the jet is narrowed; beyond the initial area of the jet the velocity of the jet q drops as the distance from the initial section increases. The jet ordinarily deflects to the surface of the water (free surface) or the bed of the channel (solid surface) by the Coanda effect and attaches to the surface at a certain section BB'; a portion of the jet turns upstream and a circulating flow occurs in front of the section BB'; the rest of the jet turns downstream and flows down with the surrounding water. When the jet attaches to the water surface, a part of the water surface rises (see Fig. 1).

There have been many studies on such flows, for example, the studies of hydraulic jump (e.g., Rajaratnam and Subramanya, 1968) and the switching mechanism of a jet in fluid control devices (e.g., Murao and Sudo, 1990). But very little is known about the details of the effect of a free and a solid surface on a water jet, as far as the authors are aware.

The purpose of this study is to investigate the flow field in an open channel formed by a water jet discharged into quiescent water and to obtain the characteristic features and quantity of the flow. To achieve this purpose, we used the methods of injecting tracer particles, dyes and hydrogen bubbles into the water.

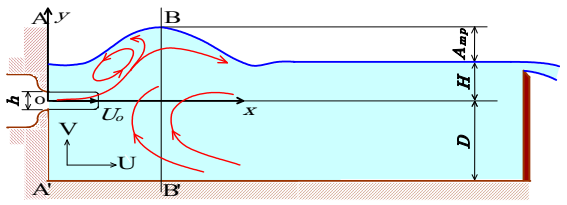

Fig. 1. Diagram of flow in an open channel.

In the following, the swell of the water surface upon the collision of the jet is referred to, for convenience, to as hydraulic jump after the hydraulic jump occurs just down an overflow and an underflow gate, although they are in essence different.

2. Experimental Apparatus and Procedure

2.1 Experimental Apparatus

Schematic diagrams of an experimental apparatus and a system of coordinates are illustrated in Fig. 2. The apparatus consists of a pipeline supplying test fluid (city water at 18℃) and a test channel. Water is delivered to a head tank mounted at about 4 meters above the test channel by a pump and is driven by a head of water. Water from the head tank passes through a control valve and a float-type flow meter, and issues horizontally from a two-dimensional contraction nozzle into the test channel. The nozzle mouth has a rectangular cross section measuring 5(height ***h***)×150(width ***B***)mm, with the aspect ratio being 30 (see Fig. 2(c)). A rectifier is installed in front of the nozzle. The test channel is made of transparent acrylic plates. Its cross section is rectangular and the interior is 150mm wide, 1200mm high and 1400mm long. A false bed is placed above the real bed of the channel and a weir is mounted at the rear end of the channel. Both are movable upward and downward and therefore the distances, ***H*** and ***D***, can be adjusted suitably to the required values, ***H*** and ***D*** denoting the vertical distance from the nozzle to the downstream water surface and to the real or false bed of the channel, respectively. In what follows, ***H*** and ***D*** are referred to as the rear water level and the depth of water. The section of the channel exceeding x=1400mm, however, is enlarged to a width of 600mm so that water flows down steadily over the weir. The flow rate of water is controlled and measured by the valve and the float-type flow meter set up below the head tank.

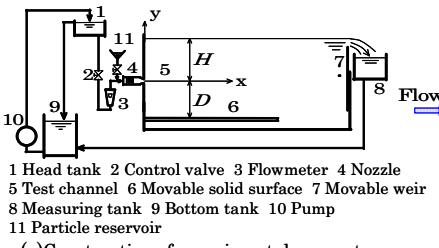

1 Head tank 2 Control valve 3 Flowmeter 4 Nozzle
5 Test channel 6 Movable solid surface 7 Movable weir
8 Measuring tank 9 Bottom tank 10 Pump
11 Particle reservoir

(a)Construction of experimental apparatus

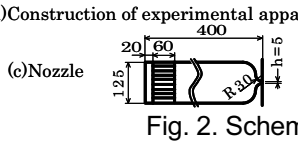

(c)Nozzle

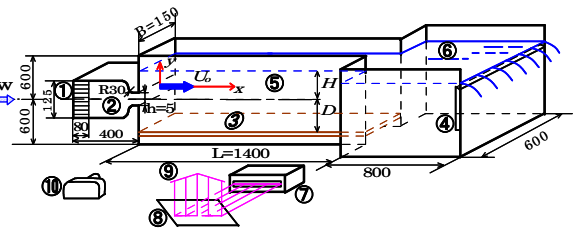

①Rectifier ②Nozzle ③Movable solid surface ④Movable weir
⑤Test channel ⑥Rear channel ⑦Light source ⑧Mirror
⑨Slit light ⑩Camera & Video

(b)Test channel and devices for visualization

Fig. 2. Schematic diagrams of experimental apparatus.

2.2 Measurement Method

In this study, the flow has been visualized by three methods using hydrogen bubbles, dye and tracer particles. The hydrogen bubble method is used to grasp the whole flow field and to classify the flow according to its mechanism, the dye injection method to clarify the flow behavior around the water surface to which the jet attaches and the tracer particle method to obtain the velocity vectors of the flow. In the hydrogen bubble method, four tungsten wires with a diameter of 100 μ m, are placed as the cathode at the center of the nozzle exit, while a fine stainless steel bar is placed as the anode in the nozzle. When the voltage of approximately 500V D.C. is applied between two poles, hydrogen bubbles arise with a roughly homogeneous density. On the other hand, in the dye injection method, the dye (red or black ink) is injected into the stream through a thin tube in the rectifier and, in the

tracer method, spherical white polystyrene particles with a diameter of about 1mm and the specific gravity of about 1.03 are added to water at the rectifier inlet. These dyes or particles are spouted from the nozzle into the test channel along with the test fluid.

The outline of the flow visualization is shown in Fig. 3. The visualization and the measurements are made on the x-y plane in the central part of the channel. In the hydrogen bubble and tracer particle method, the light from a source (150W) is transformed to a slit light of 20mm wide and thrown into the test section through the channel bed. Photographs of bubbles or tracer particles illuminated by the light are taken through a sidewall by an ordinary and a video camera. When photographing non-steady flows, the timer with accuracy of 10^{-2} seconds and the electric circuit shown in Fig. 4 are used, time being counted from the time when the hydraulic jump reaches its maximum and a switch closes. A switch is made of a thin aluminum plate and is placed, according to the preliminary experiment, such that it closes at the maximum hydraulic jump. The shutter speed of the camera is adjusted in accordance with the velocity of the flow in the test section, and the velocity vector is calculated from the length and direction of a particle path line on the photograph (Sudo et al., 1999).

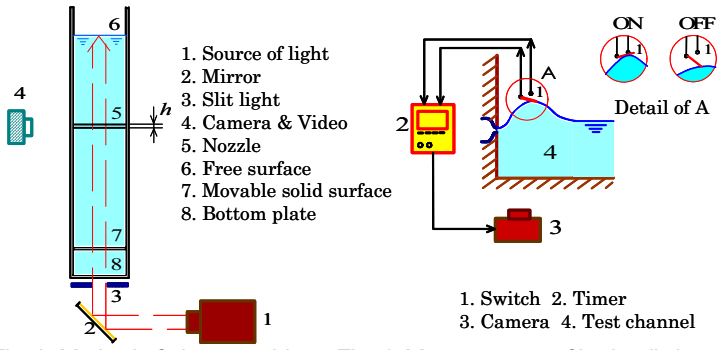

Fig. 3. Method of photographing. Fig. 4. Measurement of hydraulic jump.

2.3 Experimental Conditions and Procedure

Before the experiment, a preliminary test was conducted to check the influence of the weir and the sidewalls of the channel on the flow. It was found from the test that the weir installed at the distance x exceeding about x/h =100 does not influence the flow in the test section, and that the velocity measurement by a hot-film shows the flow to be two-dimensional in the central region of the channel.

First, the deflection direction of the jet discharged from the nozzle was examined under the condition of various rear water levels H, while the Reynolds number $Re(=U_0h/\nu$; ν : kinetic viscosity of water) and the depth of water D were fixed. Similar experiments were repeated by changing the Reynolds number and the depth of water one after another. The results show how the deflection direction and the point of attachment of the jet vary with the dynamic condition of the initial jet and the geometric condition of the flow field.

Second, the visualization of the flow was conducted in detail under various values of the Reynolds number Re, the depth of water D and rear water level H, and the relationships among the flow pattern and the dynamic and geometric conditions were examined by analyzing many photographs.

In the experiment, it was found that the jet oscillates periodically by itself and induces, in consequence, the oscillation of the water surface under a certain condition as will be mentioned later. This phenomenon was of great interest to us from the reason that this was different from the sloshing and other fluid oscillation (e.g., Okamoto et al., 1991), and so detailed photographs were taken under the conditions listed in Table 1 in order to clarify the mechanism of the self-induced vibration of the surface, that is, of the jet, Fr $(=U_0/\sqrt{gH})$ being the Froude number. These photographs enable us to understand the maximum displacement of hydraulic jump from the rear water level, A_{mp} (hereafter, referred to as the amplitude of oscillation, for convenience) and the frequency of oscillation f_z, in addition to providing a key to clarifying the mechanism of oscillation.

Table 1. Experimental conditions.

		D/h			
		20	40	60	80
Re	5000	Fr=1.84, 2.0	Fr=1.77, 1.84, 2.0	Fr=1.84, 2.0, 2.1	Fr=1.84, 2.1
	7500	Fr=2.26, 2.3, 2.4	Fr=2.3, 2.4	Fr=2.25, 2.24	Fr=2.2, 2.25, 2.4, 2.56, 2.66
	10000	Fr=2.4, 2.5, 2.6	Fr=2.5, 2.6, 2.7, 2.85	Fr=2.6, 2.7, 2.85	Fr=2.6, 2.7, 2.85, 2.9
	12500	Fr=2.8, 2.9, 3.0	Fr=2.8, 3.0, 3.1	Fr=2.9, 3.0, 3.1	Fr=2.8, 2.9, 3.0, 3.1
	15000	Fr=3.1, 3.2, 3.3, 3.4	Fr=3.1, 3.2, 3.3, 3.4	Fr=3.1, 3.2, 3.4	Fr=3.1, 3.2, 3.3, 3.4

3. Results and Discussion

3.1 Outline of the Flow Field

The jets issuing from the nozzle are classified into two types according to the deflection direction, a free jet being the exception here. As mentioned in the introduction, one is the case where the jet deflects and attaches to the water surface, and the other, where is attaches to the channel bed. Typical flows of the two types are shown in Figs. 5 and 6, respectively. In each figure, (a) is the photograph visualized by the hydrogen bubble method and (b) is the schematic diagram of streamlines.

In both cases, a clockwise or counter-clockwise circulating flow is formed in the area in front of the point of attachment, that is, of flow bifurcation, while the flow rotating in the opposite direction to the upstream circulating flow is induced in the area to the rear of the bifurcation point.

The jet attaching to the water surface shows various patterns, which are divided into six types as shown later. Any flows attaching to the channel bed, however, change their pattern only negligibly.

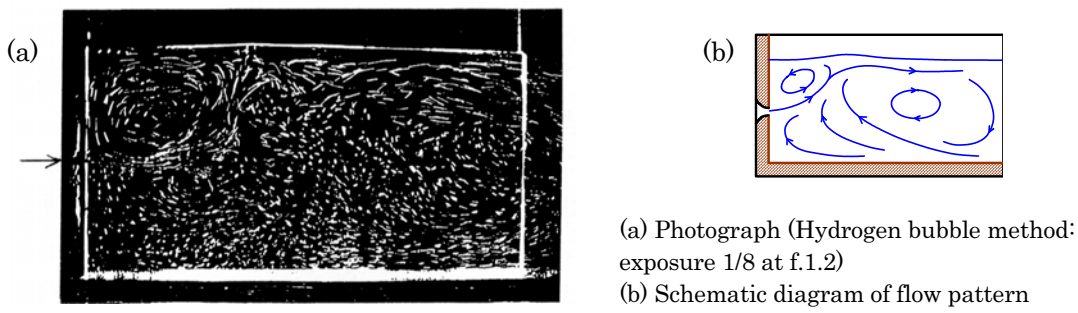

(a) Photograph (Hydrogen bubble method: exposure 1/8 at f.1.2)
(b) Schematic diagram of flow pattern

Fig. 5. Flow attaching to free surface (H/h=30, D/h=30, Re=4500).

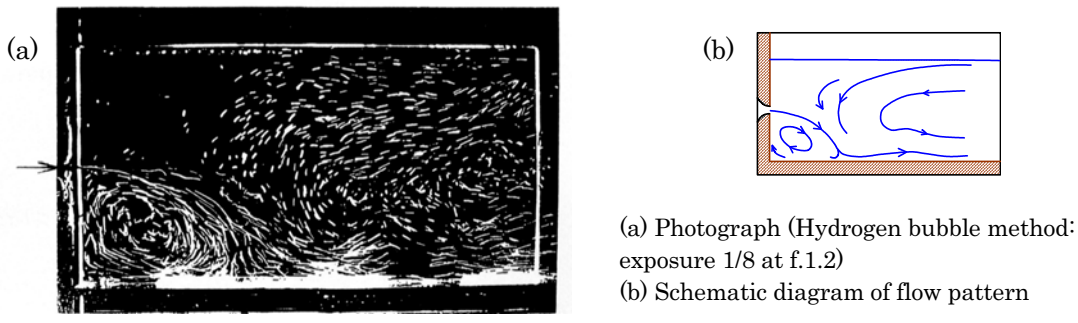

(a) Photograph (Hydrogen bubble method: exposure 1/8 at f.1.2)
(b) Schematic diagram of flow pattern

Fig. 6. Flow attaching to solid surface (H/h=30, D/h=30, Re=4500).

3.2 Deflection of the Jet

The deflection direction and the attachment point of the submerged jet must be dependant upon the dynamic condition of the jet and the geometric condition of the flow field. Figure 7 shows the influence of the rear water level H and the depth of water D on the deflection of the jet for the case of the Reynolds number Re from 2.4×10^3 to 10^4. The flow is roughly classified into three types as seen in Fig. 7:

(1) For the case where H is sufficiently larger than D, that is, for $H/h \gtrsim 2.2D/h$, the jet deflects to the channel bed and attaches to it.

(2) For the case where H is sufficiently smaller than D, that is, for $H/h \lesssim (0.27D/h+4.2)$, the jet deflects to the water surface and attaches to it.

(3) For the case where H and D are roughly parallel, that is, for $(0.27D/h+4.2) \lesssim H/h \lesssim 2.2D/h$, the deflection of the jet is not fixed.

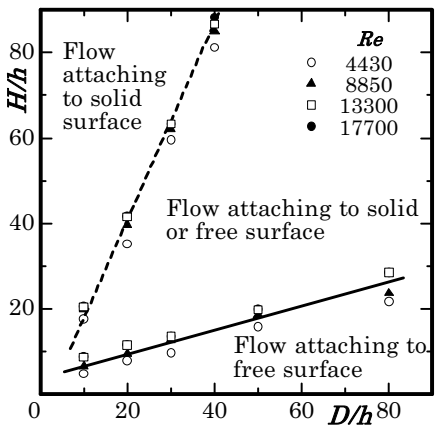

Fig. 7. Influence of H and D on deflection direction of jet (Re=2.4×10^3～10^4).

As shown in Fig. 7, the deflection direction of the jet depends significantly on ***H*** and ***D*** but only negligibly on the Reynolds number ***Re***, if anything.

3.3 Classification of the Flow Attaching to the Water Surface

3.3.1 Flow Patterns

For attaching to the water surface, the jets are propagated in different manners through the channel according to the dynamic condition of the jet and the geometric condition of the flow field, and are divided into six types according to their flow pattern.

The respective flow patterns except one are shown in Figs. 8～12. In each figure, (a) is a photograph obtained by the tracer particle method, and (b), except Fig. 12(b), is a velocity vector diagram obtained by the tracer particle method.

The outline of the respective flows is as follows:

(1) Ⅰ-type (Fig. 8): For the case where the rear water level ***H*** is at full height, the jet from the submerged nozzle deflects strongly toward the water surface and attaches to it. At this time, the water surface near the attachment point rises and the hydraulic jump occurs. In the closed area in front of the attachment point, a counter-clockwise circulating flow is induced. The jet downstream from the point of attachment flows along the water surface.

(2) Ⅱ-type (Fig. 9): For the case where the Reynolds number ***Re*** is larger and ***H*** is lower than those for the case of Ⅰ-type, the nozzle is level with the water surface and the hydraulic jump reaches higher than that for Ⅰ-type. After attaching to the water surface, the jet meanders up and down along the water surface and the water surface changes with the movement of the jet.

(3) Ⅲ-type (Fig. 10): For the case where the depth of water ***D*** is shallower than that for Ⅱ-type and the rear water level ***H*** is high, the high hydraulic jump is made and an intensive clockwise circulating flow is induced under the hydraulic jump. The jet turns downward behind the hydraulic jump and reattaches to the channel bed, and after that it flows down the channel bed.

(4) Ⅳ-type (Fig. 11): For the case where ***H*** and ***D*** are both lower than those for Ⅲ-type, the hydraulic jump decreases in scale and weakens with decreasing ***D***, and the water surface just downstream from the nozzle becomes lower than the rear water level ***H***. The jet from the nozzle shoots into the quiescent water and attaches to the channel bed. At this time, a clockwise circulating flow occurs at the front corner of the dead end of the channel and the jet moves down the channel bed.

(5) Ⅳ'-type (Fig. 12): When increasing the Reynolds number of the jet in Ⅳ-type, the water surface just downstream of the nozzle becomes even lower and a space is formed under the jet just behind the nozzle.

In any of the flows mentioned above, a weak flow that rotates in the opposite direction to the circulating flow can be induced in the area downstream from the attachment point.

(6) Ⅴ-type (Fig. 14): For the case where the jet is in between the Ⅰ- and Ⅱ-types flows, it cannot grow into a steady flow of either type. In this case, pseudo flows of Ⅰ- and Ⅱ-types appear alternately as shown in Fig. 14. Therefore, the water surface oscillates with the change of the flow type.

3.3.2 Classification of the flow

The flow pattern is expected to depend on the three parameters of the depth of water ***D***, the rear water level ***H*** and the initial velocity of the jet ***Uo***. When adopting the reduced Froude number ***Fr**** given in Eq.(1), the flow can be classified on the ***Fr**-D*** plane as shown in Fig. 13.

$$Fr^{*} = Fr \times \sqrt{\frac{h}{H}} \qquad (Fr = U_0 / \sqrt{gH}) \tag{1}$$

The flow changes from Ⅰ-type to Ⅱ-type via Ⅴ-type with the increase in ***Fr****. For the case of a small value of ***D/h***, the flow changes, however, not to Ⅱ-type but to Ⅲ-, Ⅱ- and Ⅳ-types or to Ⅲ-, Ⅳ- and Ⅳ'-types, sequentially.

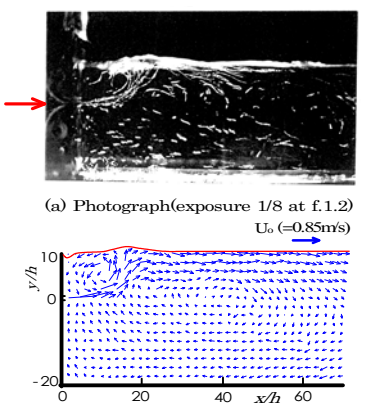

Fig. 8. Ⅰ-type
(*H*/*h*=10, *D*/*h*=20, *Re*=4000).

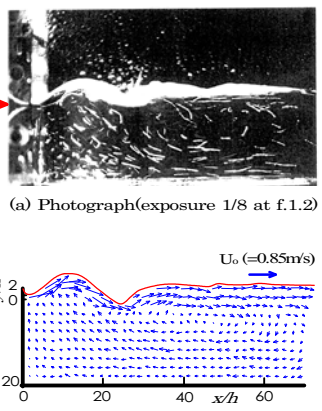

Fig. 9. Ⅱ-type
(*H*/*h*=2, *D*/*h*=20, *Re*=4000).

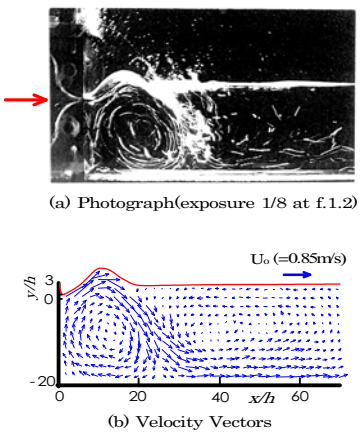

Fig. 10. Ⅲ-type
(*H*/*h*=3, *D*/*h*=20, *Re*=4000).

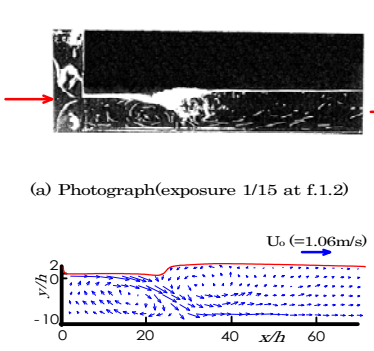

Fig. 11. Ⅳ-type
(*H*/*h*=2, *D*/*h*=10, *Re*=5000).

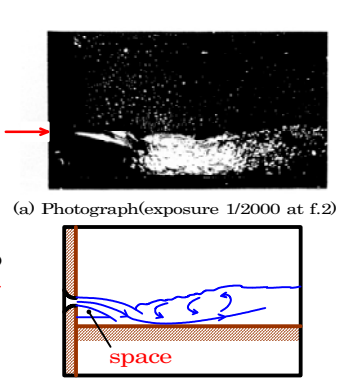

Fig. 12. Ⅳ'-type
(*H*/*h*=0.5, *D*/*h*=10, *Re*=8000).

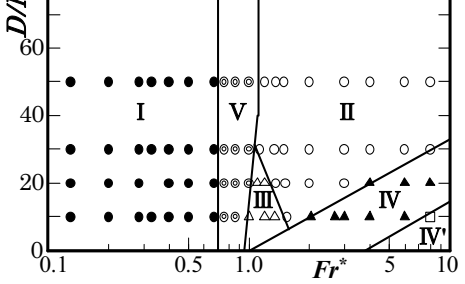

Fig. 13. Classification of flow patterns
(Symbols: experimental data).

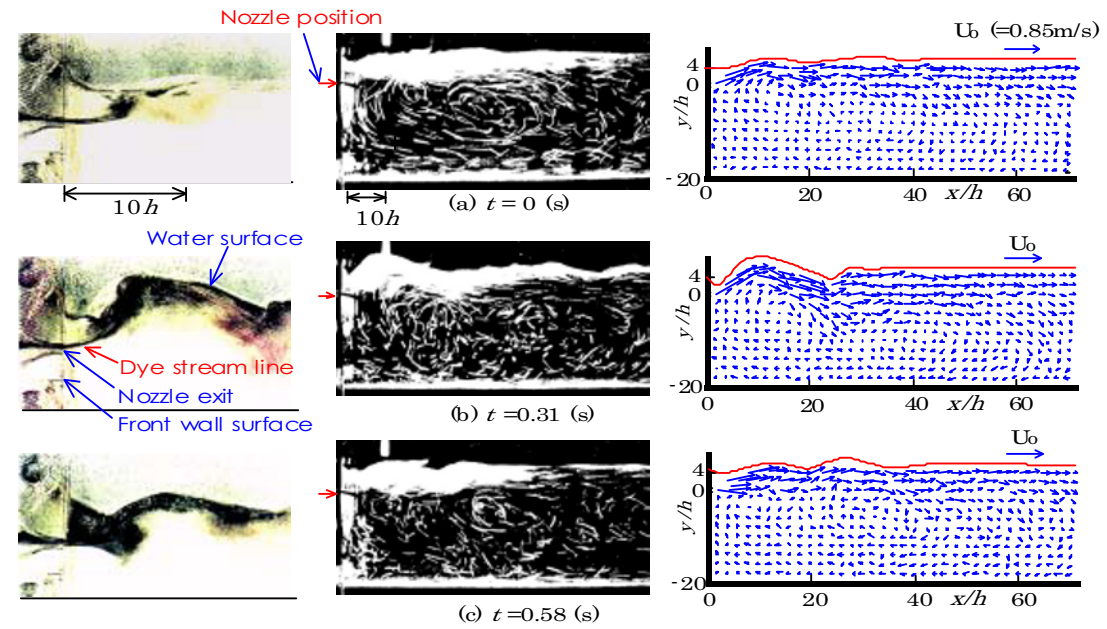

(1) Photograph (Dye injection streak line method: exposure 1/60 at f.1.4)
(2) Photograph (Tracer particle method: exposure 1/8 at f.1.2)
(3) Velocity vectors

Fig. 14. Typical example of self-induced vibration of free surface, i.e., jet.

3.4 Self-induced Vibration of the Jet, i.e., the Water Surface

3.4.1 Outline of the Flow Field

The result for Re=4000, H/h=4 and D/h=20 is chosen here as a representative example. Figures 14(1) and (2) are successive photographs of typical fluid motion as obtained by the dye injection and tracer particle methods, with t being measured from the time when the water surface had recovered its initial level. Figure 14(3) shows the velocity vectors of the flow corresponding to the middle photographs.

3.4.2 Mechanism of Self-induced Vibration of the Jet

A discussion is presented on the occurrence and mechanism of self-induced vibration of the water surface, i.e., the jet, in the following (with reference to Fig. 15):

(1) The jet discharged horizontally from the nozzle reaches the water surface at a certain distance downstream from the nozzle. At this time, the water surface is roughly even over the entire range of the test section [Fig. 15(a)].

(2) The pressure in region A shown in the schematic diagram lowers since the jet entrains the water in this region. Consequently, the jet deflects to the water surface, and this phenomenon is known as the Coanda effect. The water surface rises with the deflection of the jet and the hydraulic jump is formed [Fig. 15(b)].

(3) The water surface of region A goes down with the lapse of time. The deflection of the jet makes rapid progress, and finally the level of the jump reaches its highest point [Fig. 15(c)].

(4) When the jump reaches its maximum, the jet bifurcates before and behind the attachment point S. The water level of region A increases gradually due to the supply of water by the bifurcation and the pressure in this region rises [Fig. 15(d)].

(5) The pressure rise in region A reduces the Coanda effect and the deflection of the jet becomes weaker. Consequently, the attachment point of the jet moves away from the nozzle and the swell of the water surface falls to the initial level [Fig. 15(e)].

(6) The above-mentioned process is repeated.

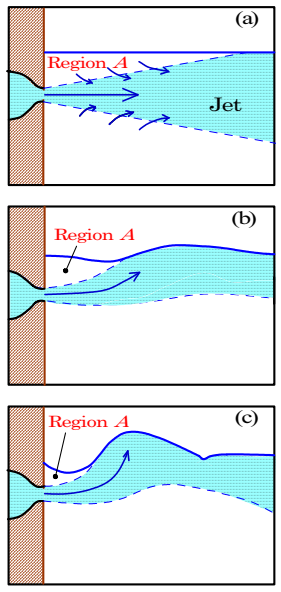

Fig. 15. Schematic diagram of flow mechanism.

3.4.3 Characteristics of Vibration of the Water Surface, i.e., the Jet

The frequency and amplitude of oscillation of the water surface, f_z and A_{mp}, which are the arithmetical averages of the results obtained through many trials, are plotted against the rear water level H in Figs. 16 and 17, respectively. In each figure, (a) shows the results for the various Reynolds numbers and a fixed depth D/h=80, while (b) shows the results for the case of D/h=20 in which the channel bed has a slight influence on the flow.

As known from Fig. 16, the frequency f_z is independent of H and decreases with increasing the Reynolds number. The mutual relationship of f_z to H or Re is explained as follows: When H is high, region A is large and so it takes a long time for the pressure in the region to lower, due to the entrainment by the jet. The pressure in region A, however, increases rapidly after the bifurcation of the jet because of the large volume of the back-flowing jet. When H is low, the bifurcation of the jet begins in a short time, but the pressure rise in region A occurs slowly because the deflection angle of the jet is small in this case and the volume of the back-flowing jet decreases. Regarding the Reynolds number, the entrainment by the jet becomes stronger according to an increase in Re and so it takes a longer time for the volume of water in region A to recover due to the back-flowing jet. This causes the decrease of frequency f_z, but f_z depends only negligible on Re for $Re \gtrsim 10000$.

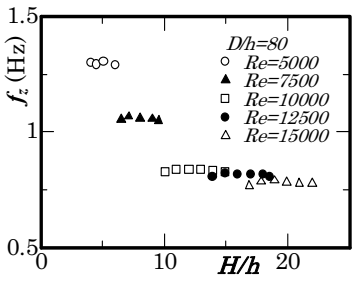

(a)

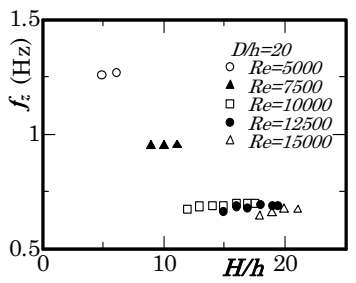

(b)

Fig. 16. Frequency of vibration of hydraulic jump.

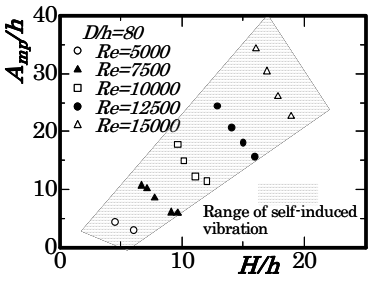

(a)

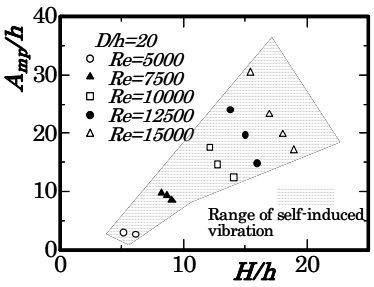

(b)

Fig. 17. Amplitude of hydraulic jump.

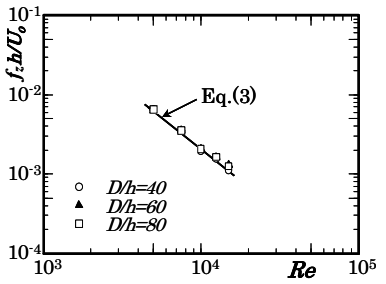

Fig. 18. Frequency of vibration of hydraulic jump.

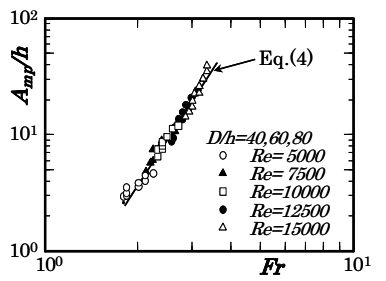

Fig. 19. Amplitude of hydraulic jump.

The amplitude of oscillation A_{mp} decreases with an increase in the rear water level H for a fixed Reynolds number Re because the jet, for high H, loses most of the energy necessary for the hydraulic jump before arriving at the water surface. It can be explained from the similar discussion that the amplitude increases with the Reynolds number.

The dimensional analysis gives the following equations relative to f_z and A_{mp} for the case of $D/h \gtrsim 30$ where the oscillation of the jet is not under the influence of the channel bed:

$$\frac{f_z \cdot h}{U_0} = F_1(Re) \ , \quad \frac{A_{mp}}{h} = F_2(Fr) \ , \tag{2}$$

Here $Re = U_0 h / \nu$ and $Fr = U_0 / \sqrt{gH}$. Equation (2) is written by determining the functions F_1 and F_2 with the aid of the experimental results:

$$\frac{f_z \cdot h}{U_0} = 2200 R_e^{-1.5} \qquad (Re \fallingdotseq 5000 \sim 15000, \ D/h \gtrsim 30) \ , \tag{3}$$

$$\frac{A_{mp}}{h} = 0.25 Fr^4 \qquad (Fr \fallingdotseq 1.7 \sim 3.3, \ D/h \gtrsim 30) \ . \tag{4}$$

4. Conclusion

Two-dimensional submerged water jets were examined experimentally by various methods of visualization. The jet is deflected to the free or solid surface by the Coanda effect after issuing from the nozzle.

The jet that deflects to the free surface was classified into six types and a classification map was drawn on the Fr^*-D/h plane.

One interesting phenomenon, which the jet under a certain condition, which corresponds to one of six types, oscillates by itself, was observed and the mechanism of the self-induced vibration of the jet was clarified by analyzing many photographs.

References

Murao, T. and Sudo, K., Switching Mechanism of a Jet in a Wall-Attachment Device, Trans. of JSME, 56-531, B (1990), 3360-3365.

N. Rajaratnam and K. Subramanya, Hydraulic Jumps Below Abrupt Symmetrical Expansions, Journal of the Hydraulics Division Proceedings of the American Society of Civil Engineers, 94-HY2 (1968), 481-503.

N. Rajaratnam and S. Subramanyan, Plane Turbulent Buoyant Surface Jets and Jumps, Journal of Hydraulic Research, 23-2 (1985), 131-146.

N. S. Govinda Rao and N. Rajaratnam, The Submerged Hydraulic Jump, Journal of the Hydraulics Division Proceedings of the American Society of Civil Engineers, 89-HY1 (1963), 139-163.

Okamoto, K., Madarame, H. and Hagiwara, T., Self-Induced Oscillation of Free Surface in a Tank with Circulating Flow (1st Report, Experimental Results), Trans. of JSME, 57-535, C (1991), 647-653.

Shakouchi, T., Hirai, K., Fujita, K. and Ando, T., Self-Induced Oscillation of Three-Dimensional Turbulent Jet Issued into Open Channel, Trans. of JSME, 62-594, B (1996), 527-532.

Someya, S., Okamoto, K. and Madarae, H., The Self-Induced Free-Surface "Swell Flapping" caused by the interaction among a jet, a free surface and a structure, Journal of Fluids and Structures, 14-4 (2000), 511-528.

Sudo, K., Sumida, M., Hibara, H. and Harada, M., Characteristics of Plane Submerged Water Jets Influenced by Boundaries, Journal of Visualization Society of Japan, 19-72 (1999), 25-33.

Thomas F. Swean Jr., Steven E. Ramberg, Michael W. Plesniak and Michael B. Stewart, Turbulent Surface Jet in Channel of Limited Depth, The Journal of Hydraulic Engineering, 115-12 (1989), 1587-1606.

Author Profile

Shimada Nobukazu: He received the M.Sc (Mercantile Marine) degree in 1983 from Tokyo University of Mercantile Marine. After obtaining the M.Sc. degree he became a lecturer at the Japan Coast Guard Academy. Then he went on to Hiroshima University to study, and received the D.Eng. degree in 2001 from the same university. Currently he works as a professor at J.C.G.A. His research interests include the flow visualization and self-induced vibration phenomenon of submerged water jets.

Hibara Hideki: He obtained the M.Eng. degree in 1990 from Hiroshima University. Since then, serving as a research associate, he has worked on the interaction between jets and boundary surfaces, and received the D.Eng. degree in 1998 from Hiroshima University. Currently he is working as an associate professor at Ehime University. His research interests include the control of jets and the flow structures in various pipe flows.

Ishibashi Yukio: He received the D.Eng. degree in 1989 from the Science University of Tokyo. He devoted himself to the study of fluid dynamics at the Tokyo Institute of Technology from 1969 to 1991. He moved to Chiba Polytechnic College as an associate professor in 1991 and works now as a professor. He has academic achievements in the areas of electromagnetic and ferromagnetic fluid dynamics, in addition to jet dynamics.

Sumida Masaru: He received the M.Eng. degree from the Tokyo Institute of Technology in 1977. He received the D.Eng. degree in Mechanical Engineering in 1990 from Hiroshima University. He has worked in the Department of Mechanical System Engineering, Hiroshima University, since 1996. His research interests include the flow visualization and unsteady (oscillating and pulsating) flows in pipes and ducts.

Sudo Kozo: He received the M.Eng. degree in 1964 and the D.Eng. degree in 1975 from the Tokyo Institute of Technology. He worked as a research associate at the Tokyo Institute of Technology from 1968 to 1980, and moved to Hiroshima University as an associate professor in 1980. He is now a professor emeritus of Hiroshima University and works as a professor at the Shibaura Institute of Technology.